Role of near-surface environment in tuning electrochemical CO2 reduction reaction and H2 evolution reaction

Goyal, A.G.

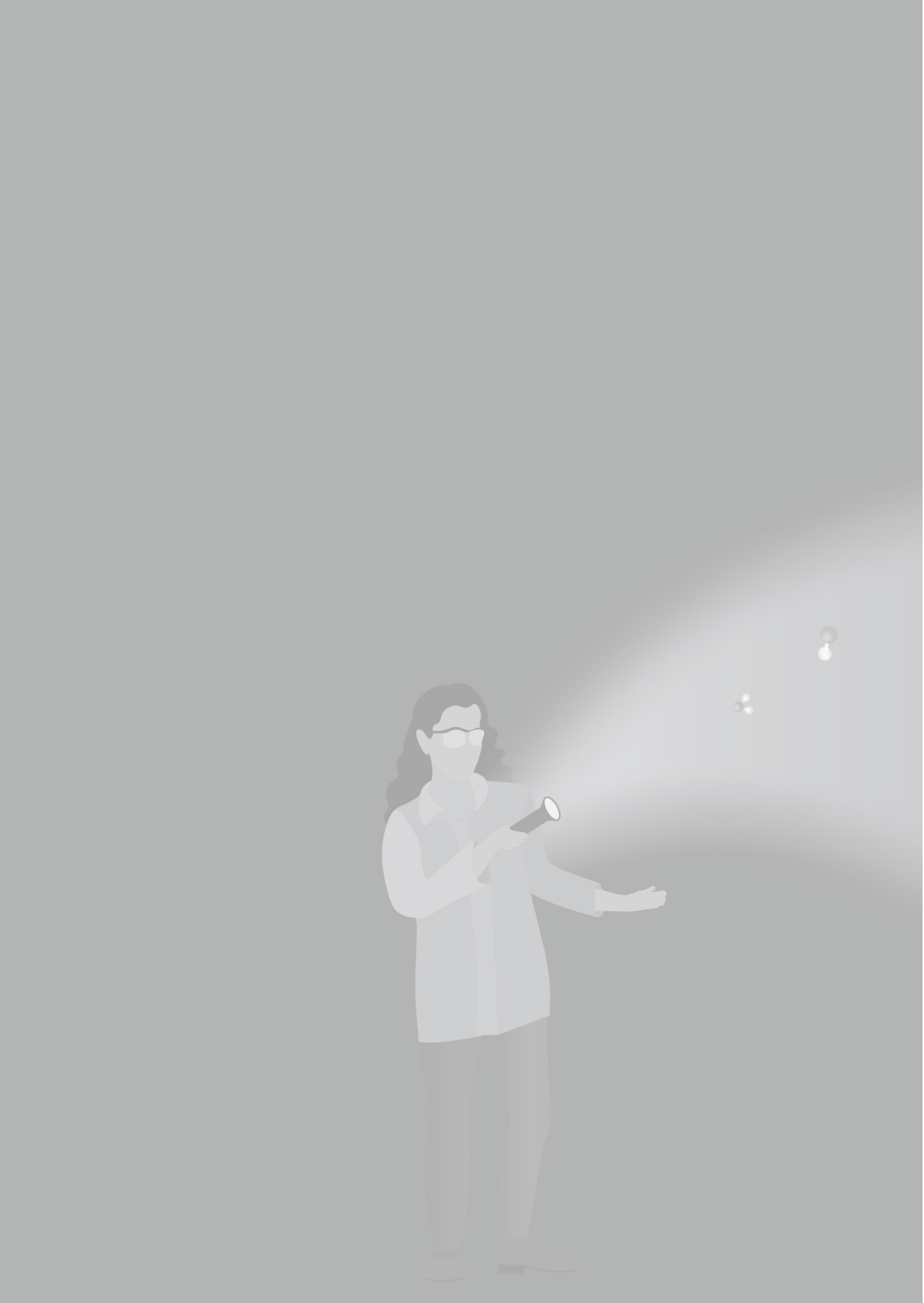

Appendix A

Supporting Information to Chapter 2

This is available as the Supporting Information to the article:
Goyal, A.; Marcandalli, G.; Mints, V. A.; Koper, M. T. M., Competition between CO_2 Reduction and Hydrogen Evolution on a Gold Electrode under Well-Defined Mass Transport Conditions. *Journal of the American Chemical Society* **2020,** *142* (9), 4154-416

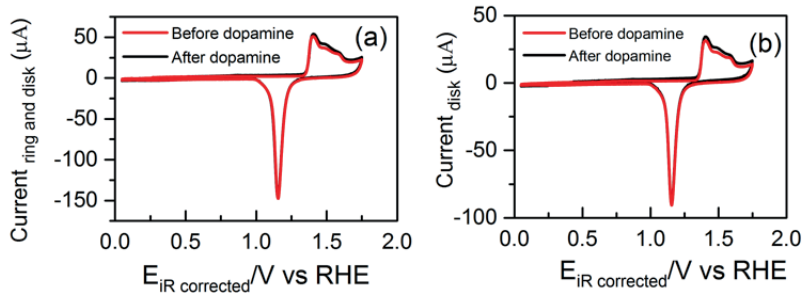

FigureS1 Characterization CV of (a) Ring and Disk and (b) Disk, in 0.1 m H_2SO_4, recorded at 50 mVs^{-1}. Red: before dopamine coating. Black: after dopamine coating.

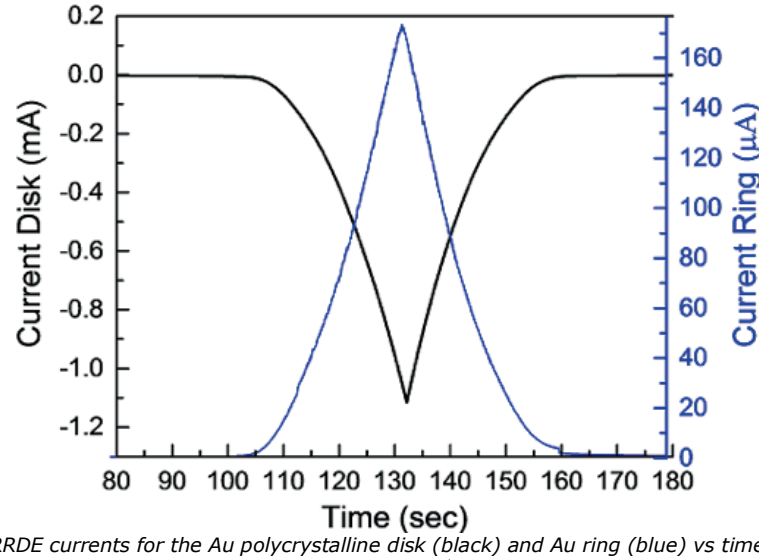

FigureS2 RRDE currents for the Au polycrystalline disk (black) and Au ring (blue) vs time, in CO_2 sat. 0.1 M $NaHCO_3$ (bulk pH =6.8), recorded at 25 mVs^{-1} at 800 rpm.

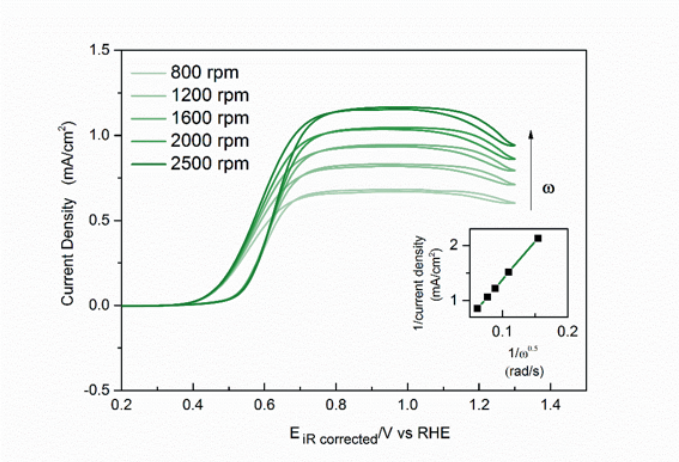

Figure S3 CO oxidation CV on Au polycrystalline surface at different rotation rates in CO sat. 0.1 M $NaHCO_3$ (bulk pH = 9), recorded at 25 mVs^{-1} from 0.2 V to 1.3 V vs RHE. The direction of the arrow indicates increasing rotation rate. Inset shows the Koutecky-Levich analysis for the CO oxidation currents at 1 V (vs RHE), where the calculated intercept of the line is 0.006.

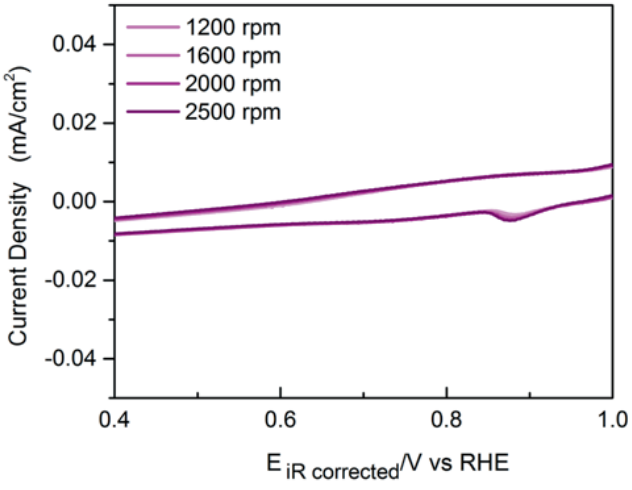

FigureS4 CV for Au polycrystalline surface in H_2 sat. 0.1 M $NaHCO_3$ (bulk pH = 9) in the potential window of CO oxidation recorded at 25 mVs^{-1}, at different rotation speeds.

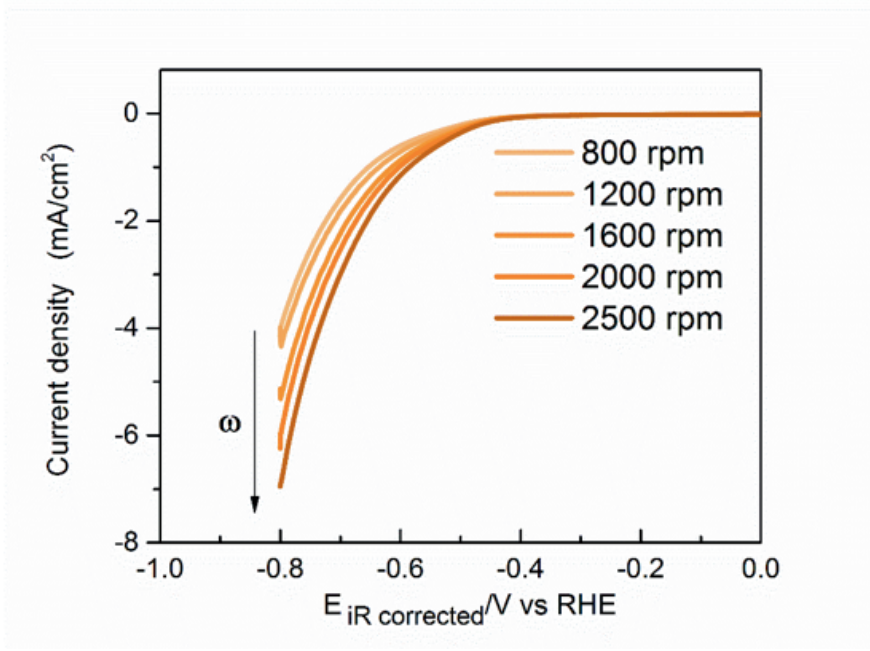

FigureS5 CVs obtained for HER at different rotation rates using the RDE on Au polycrystalline surface in Ar sat. 0.5 M $NaHCO_3$ at 25 mVs^{-1}. The direction of the arrow indicates increasing rotation rate.

Table S3 Theoretically calculated diffusion limited currents for the two electron CO_2 reduction in the RDE set-up at different rotation rates, by using the Levich equation and Fick's first law of diffusion. Where diffusion coefficient of CO_2 is taken to be 1.6 X 10^{-5} cm^2/s, the kinematic viscosity of water is taken to be 8.9 X 10^{-3} cm^2/s, the Faraday's constant is taken to be 96500 C/mol, the number of electrons involved is taken to be 2 and the concentration of CO_2 in the bulk is taken to be 33 mM.[1-2]

Rotation speed (rpm)	Diffusion layer thickness (µm)	J limiting theoretical (mA/cm^2)
400	2.7	-36.6
800	1.9	-51.8
1200	1.6	-63.4
1600	1.4	-73.2
2000	1.3	-81.9
2500	1.1	-91.5

References

1.Bard, A. J.; Faulkner, L. R., *Electrochemical methods : fundamentals and applications* Wiley: New York, **1980**.

2.Ooka, H.; Figueiredo, M. C.; Koper, M. T. M., Competition between Hydrogen Evolution and Carbon Dioxide Reduction on Copper Electrodes in Mildly Acidic Media. *Langmuir* **2017**, *33* (37), 9307-9313.

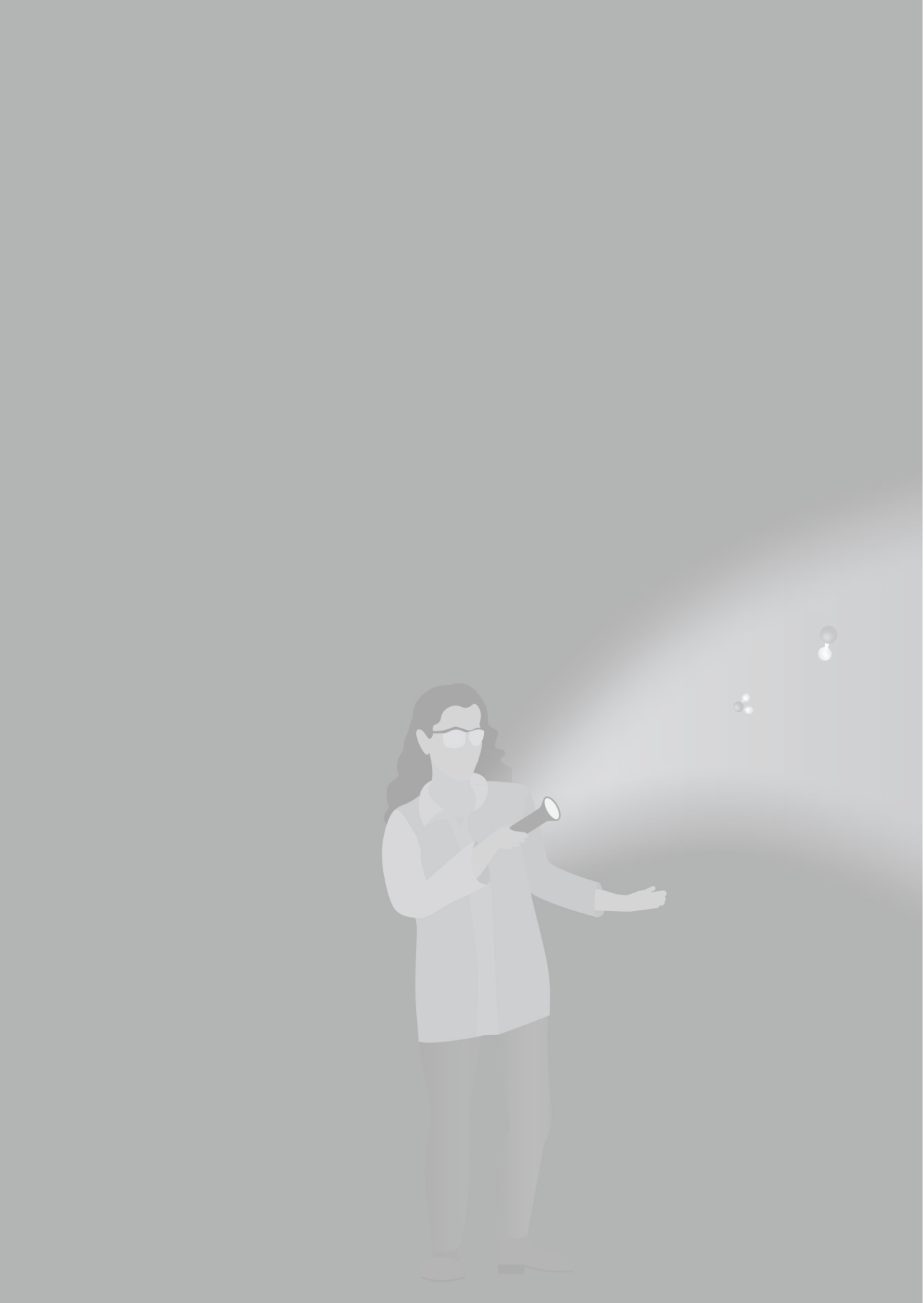

Appendix B
Supporting Information to Chapter 3

This is available as the Supporting Information to the article:
Goyal, A.; Koper, M. T. M., The Interrelated Effect of Cations and Electrolyte pH on the Hydrogen Evolution Reaction on Gold Electrodes in Alkaline Media. *Angewandte Chemie International Edition* **2021,** *60* (24), 13452-13462

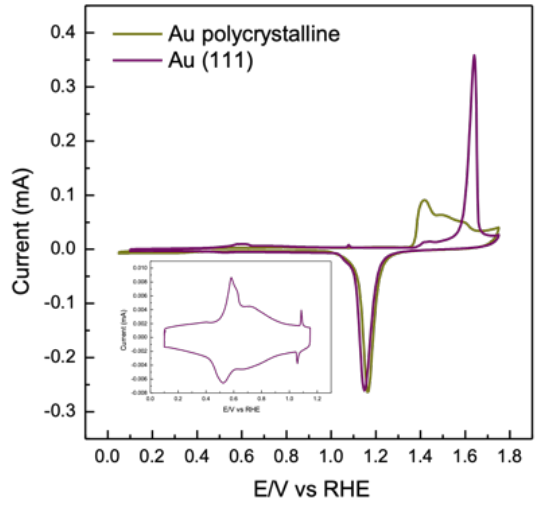

Figure S1 Characteristic cyclic voltammograms for Au polycrystalline surface (golden) and Au(111) surface (purple) obtained in 0.1 M H_2SO_4 in Ar sat. environment at 50 mVs^{-1}. The inset shows the characteristic double-layer features of the Au(111) surface in the potential window of 0.1 V to 1.15 V (vs RHE).

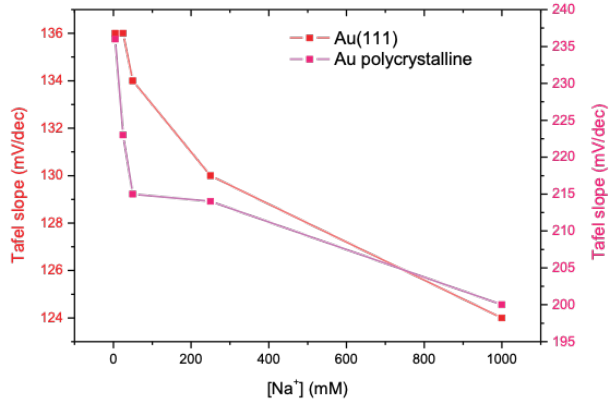

Figure S2 Tafel slopes obtained for Au polycrystalline surface (pink; right hand side on the y-axis) and Au(111) surface (red; left hand side on the y-axis) at pH 11 for different Na^+cation concentration in the electrolyte (plotted on the x-axis). The data is obtained from the steady-state currents obtained at 50 mV potential steps in the HER region.

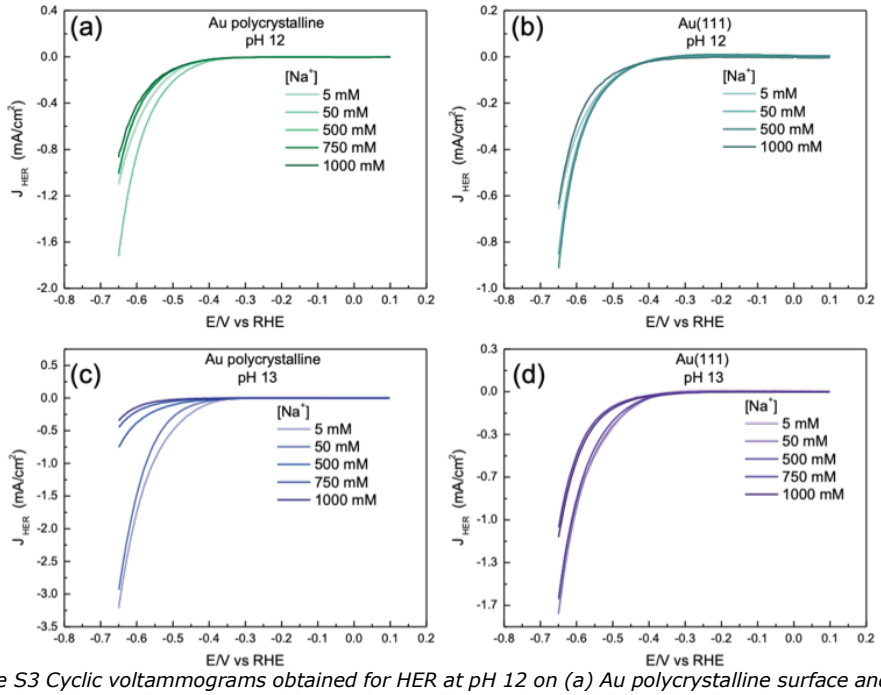

Figure S3 Cyclic voltammograms obtained for HER at pH 12 on (a) Au polycrystalline surface and (b) Au(111) surface and at pH 13 on (c) Au polycrystalline surface and (d) Au(111) surface at 2500 rpm for different concentrations of $NaClO_4$ (5 mM, 50 mM, 500 mM, 750 mM and 1000 mM) in Ar sat. environment at 25 mVs^{-1}.

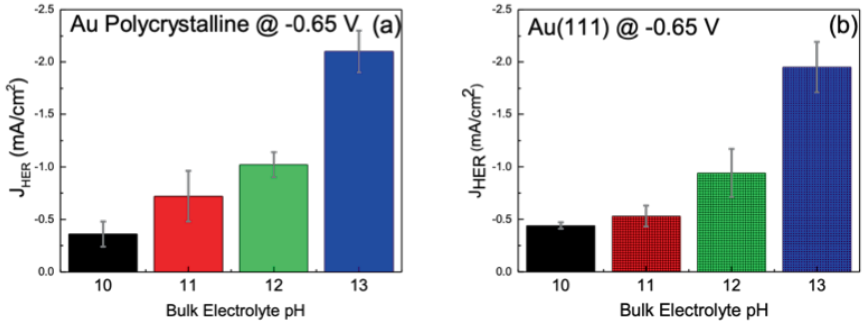

Figure S4 Characteristic current densities obtained for (a) Au polycrystalline surface and (b) Au(111) surface in 0.1 M electrolytes at different bulk pH (pH 10 to pH 13) in Ar sat. environment at - 0.65 V (vs RHE) at 2500 rpm.

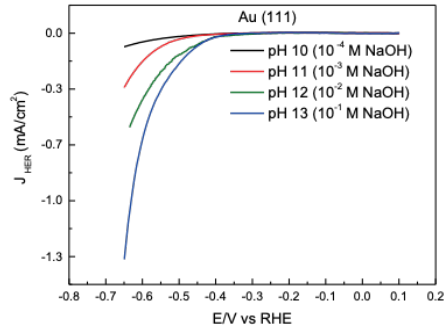

Figure S5 Cyclic voltammograms obtained for HER on Au(111) surface in 0.1 M NaOH (pH 13), 0.01 M NaOH (pH 12) , 0.001 M NaOH (pH 11) and 0.0001 M NaOH (pH 10), in Ar sat. environment at 25 mVs^{-1} under stationary hanging meniscus configuration. In these experiments the ionic strength of the electrolyte is not fixed.

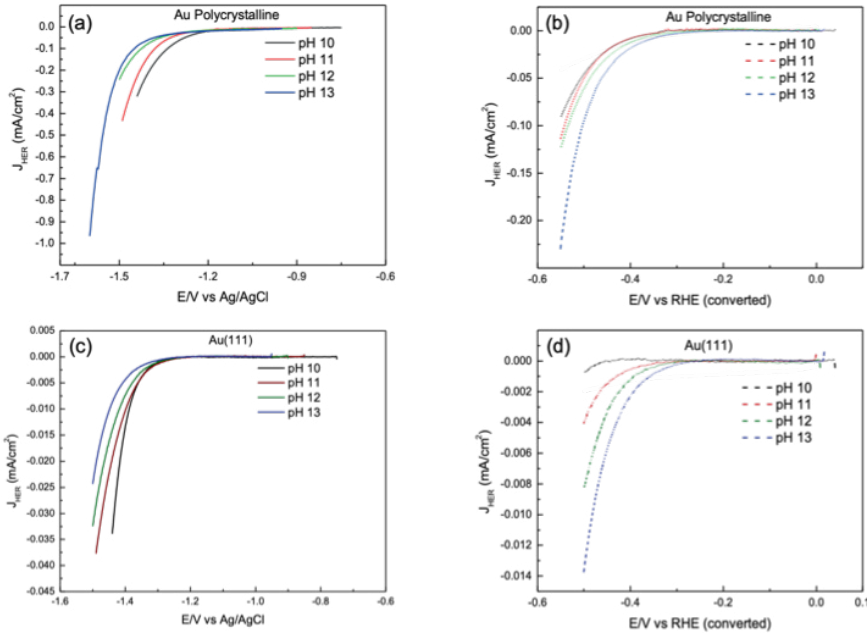

Figure S6 Cyclic voltammograms obtained for HER on (a) Au polycrystalline surface and (c) (d) Au(111) surface at 2500 rpm in 0.1 M NaOH (pH 13), 0.01 M NaOH +0.09 M $NaClO_4$ (pH 12) , 0.001 M NaOH + 0.099 M $NaClO_4$ (pH 11) and 0.0001 M NaOH +0.0999 M $NaClO_4$ (pH 10), in Ar sat. environment at 25 mVs^{-1} with a Ag/AgCl reference and in (b), (d) the data is plotted on the RHE scale where the potentials are converted post experiment from (a) and (c) respectively.

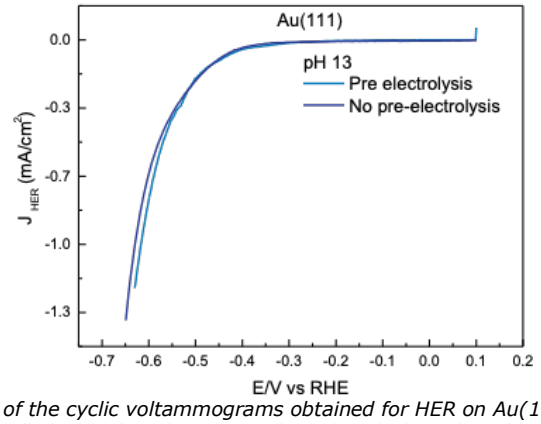

Figure S7 Comparison of the cyclic voltammograms obtained for HER on Au(111) surface in the pre-electrolyzed electrolyte (light blue) and non-pre-electrolyzed electrolyte (dark blue) at pH 13 in Ar sat. environment at 25 mVs^{-1}.

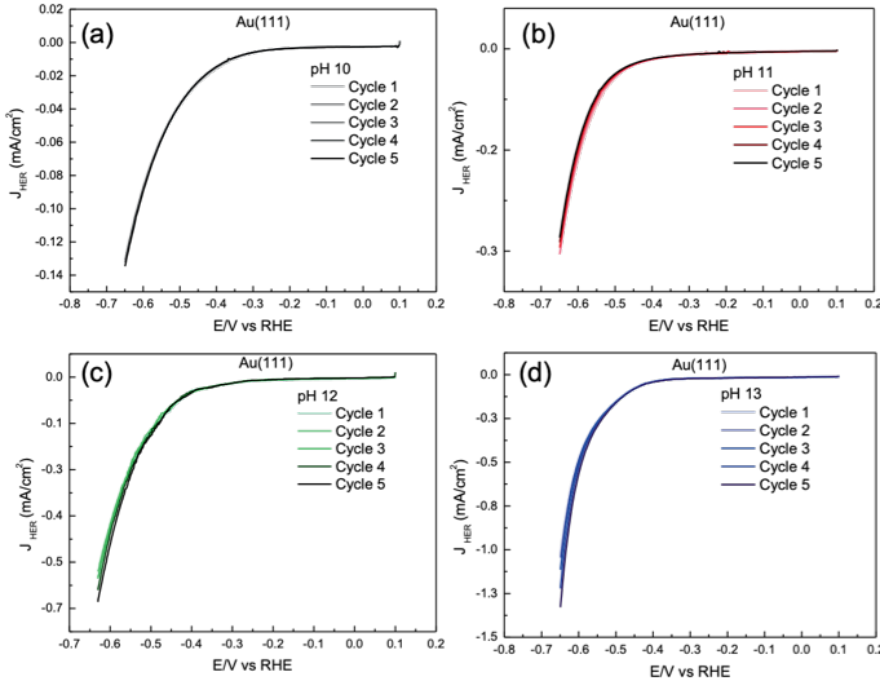

Figure S8 First five cycles of the cyclic voltammograms obtained for HER on Au(111) surface at (a) pH 10, ,(b) pH 11, (c) pH 12 and (d) pH 13 in Ar sat. environment at 25mVs^{1}.

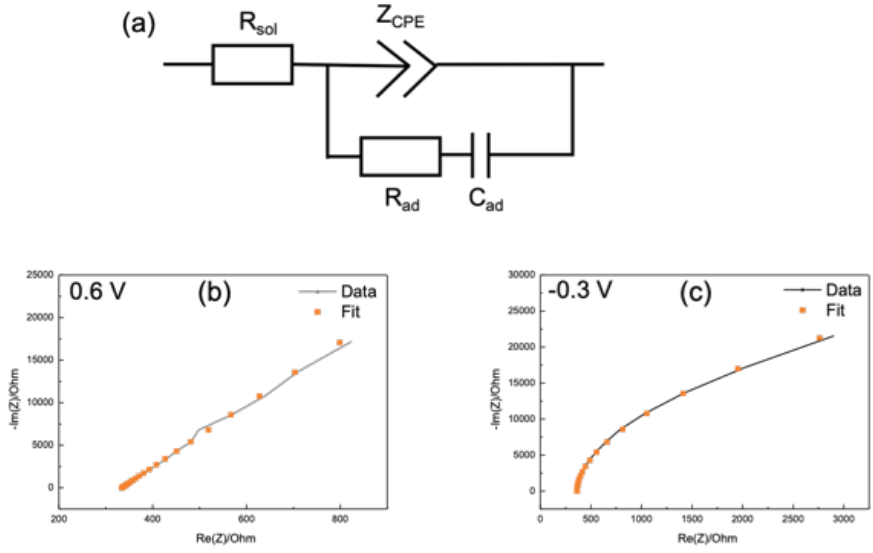

Figure S9 Typical EIS data plotted in the Nyguist impedance representation where the fits are obtained with the equivalent electric circuit (EEC) shown in (a) and the plots obtained at pH 10 in the (b) double layer region (0.6 V) and (c) near HER region (-0.3 V) are shown for comparison. In general, it was observed that in the double layer, where no Faradaic processes happen, R_{ad} and C_{ad} terms could be neglected as the main contribution in the overall capacitance came from the Z_{CPE} (Z_{CPE} = $C'_{dl}{}^{-1}(j\omega)^{-n}$) term whereas near the onset of HER the constant phase (n) for Z_{CPE} became quite low (around 0.5), thereby losing any real physical meaning and the main contribution in the overall capacitance came from the C_{ad} term.

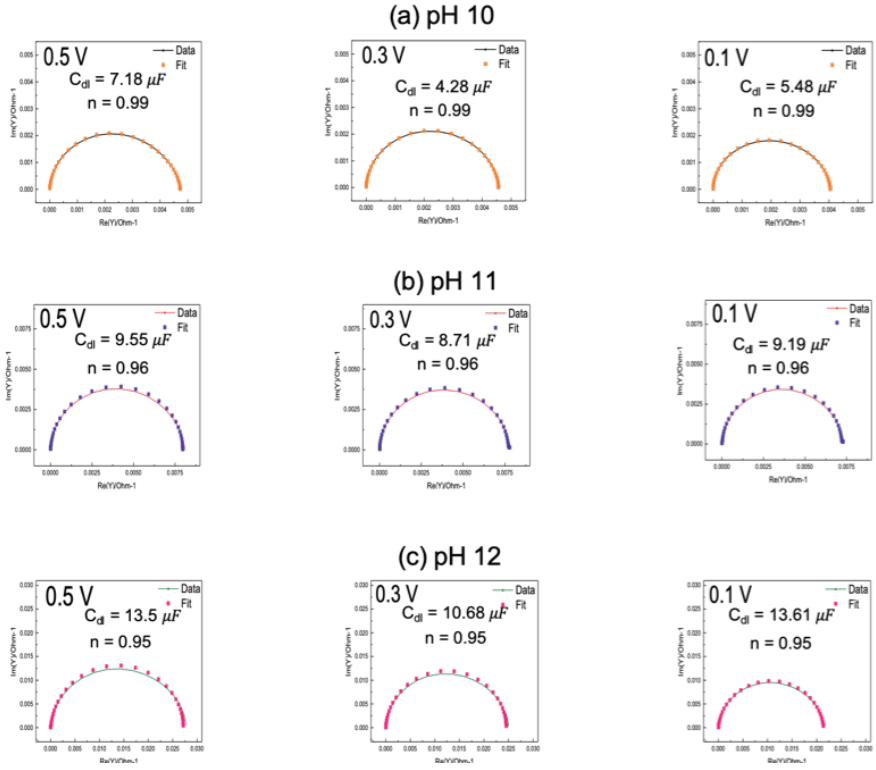

Figure S10 Typical Nyguist admittance plots and the fits obtained from the EIS data in the double layer region (0.5 V, 0.3 V and 0.1 V; left to right) at (a) pH 10, (b) pH 11 and (c) pH 12 where the EEC used to fit the data is the same as shown in Figure S10a. The value of the double layer capacitance (C_{dl}) and the CPE exponent term (n) as obtained from the Z_{CPE} ($Z_{CPE} = C'_{dl}{}^{-1}(j\omega)^{-n}$; it is assumed that *$C'_{dl}$ represents the true double layer capacitance (C_{dl}) in the limit of n ≥ 0.95) term are indicated in the graph where it is observed that the value of C_{dl} increases from pH 10 to pH 12 and the value of n decreases from pH 10 to pH 12. At pH 13 (data not shown) the EEC showed a significant contribution from the C_{ad} term in the double layer such that the exponent term of the double layer capacitance became quite low (n < 0.9), thus making it difficult to derive any real physical meaning from the Z_{CPE} term in the double layer.*

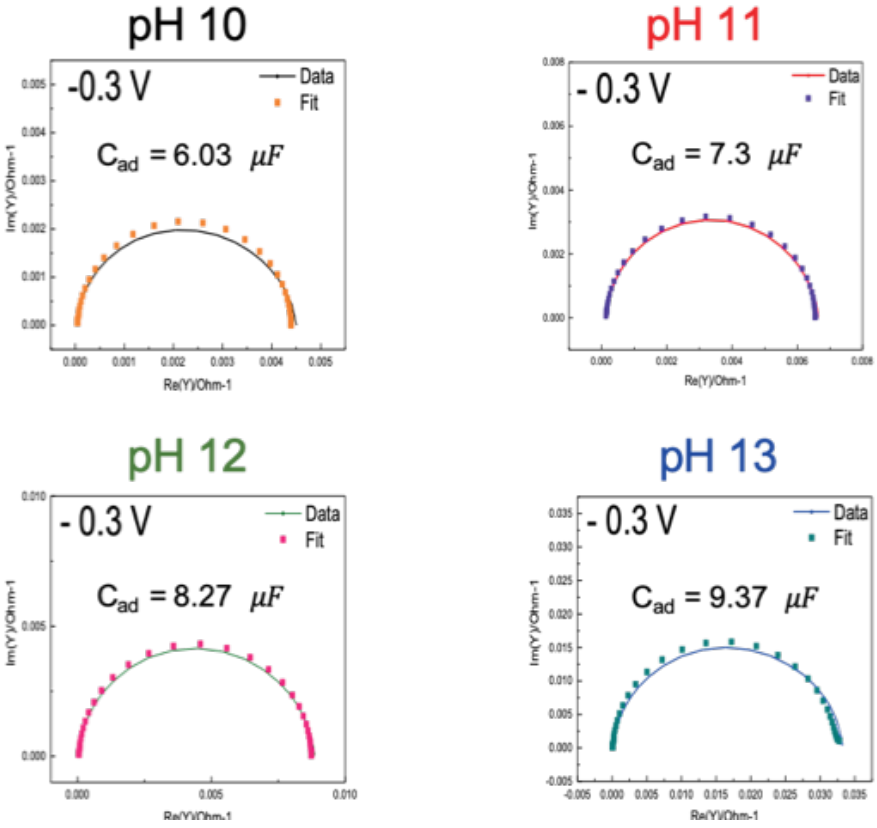

Figure S11 Typical Nyguist admittance plots and the fits obtained from the EIS data in the near HER region (-0.3 V) at pH 10, pH 11, pH 12 and pH 13 where the EEC used to fit the EIS data is same as Figure S11 (a). In the near HER region, the CPE term (Z_{CPE}) representing the double layer capacitance shows very low values for the exponent term (around 0.5) and hence cannot be used to derive any physical meaning. In this region contribution from the C_{ad} (adsorption capacitance) term becomes significant such that the value of C_{ad} increases form pH 10 to pH 13. The value for the C_{ad} obtained through the fits is indicated in the admittance plots.

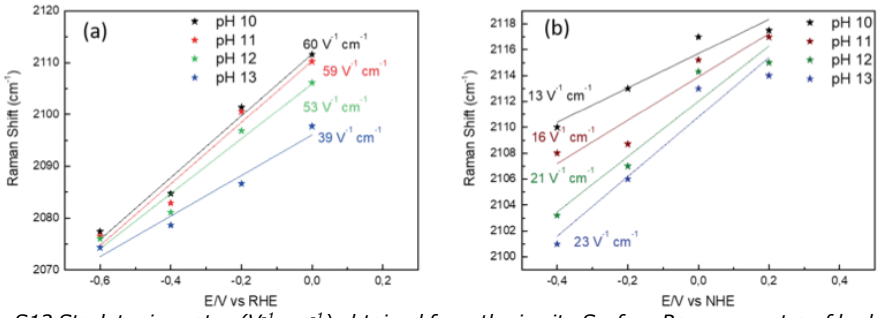

Figure S12 Stark tuning rates (V^{-1} cm^{-1}) obtained from the in situ Surface Raman spectra of hydrogen adsorption on roughened Au polycrystalline electrode on the (a) RHE scale and (b) NHE scale in 0.1 M NaOH (pH 13), 0.01 M NaOH +0.09 M $NaClO_4$ (pH 12) , 0.001 M NaOH + 0.099 M $NaClO_4$ (pH 11) and 0.0001 M NaOH +0.0999 M $NaClO_4$ (pH 10), in Ar sat. environment.

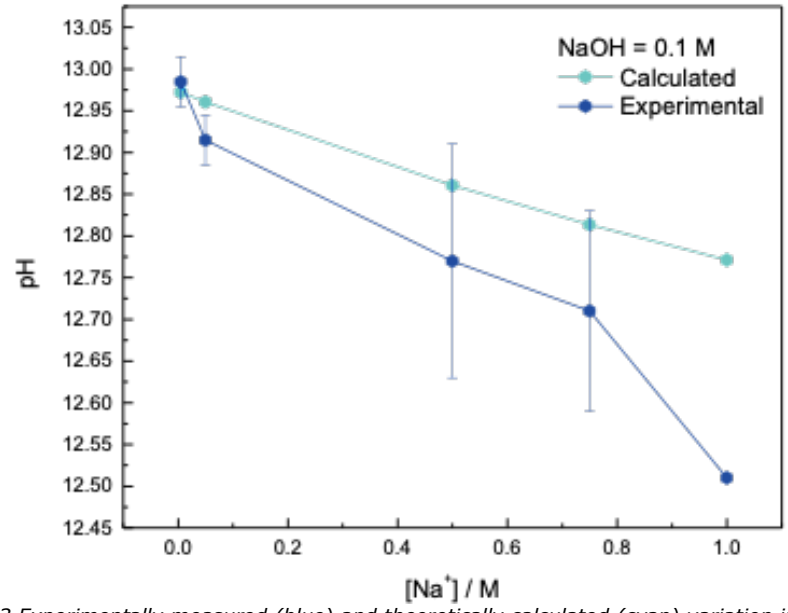

Figure S13 Experimentally measured (blue) and theoretically calculated (cyan) variation in the bulk pH in a 0.1 M NaOH electrolyte with the changing Na^+ cation concentration in the electrolyte (5mM, 50 mM, 500 mM, 750 mM and 1000 mM). For calculating the bulk pH, $pK_{hydrolysis}$ of the Na^+ cation was taken to be 14.2. The discrepancy between the experimentally observed pH and the theoretically calculated pH most likely arises from the changes in the local pH of the electrolyte which are not taken into account in the theoretical calculation of the pH.[1]

References

1. Singh, M. R.; Kwon, Y.; Lum, Y.; Ager, J. W.; Bell, A. T., Hydrolysis of Electrolyte Cations Enhances the Electrochemical Reduction of CO2 over Ag and Cu. *Journal of the American Chemical Society* **2016,** *138* (39), 13006-13012.

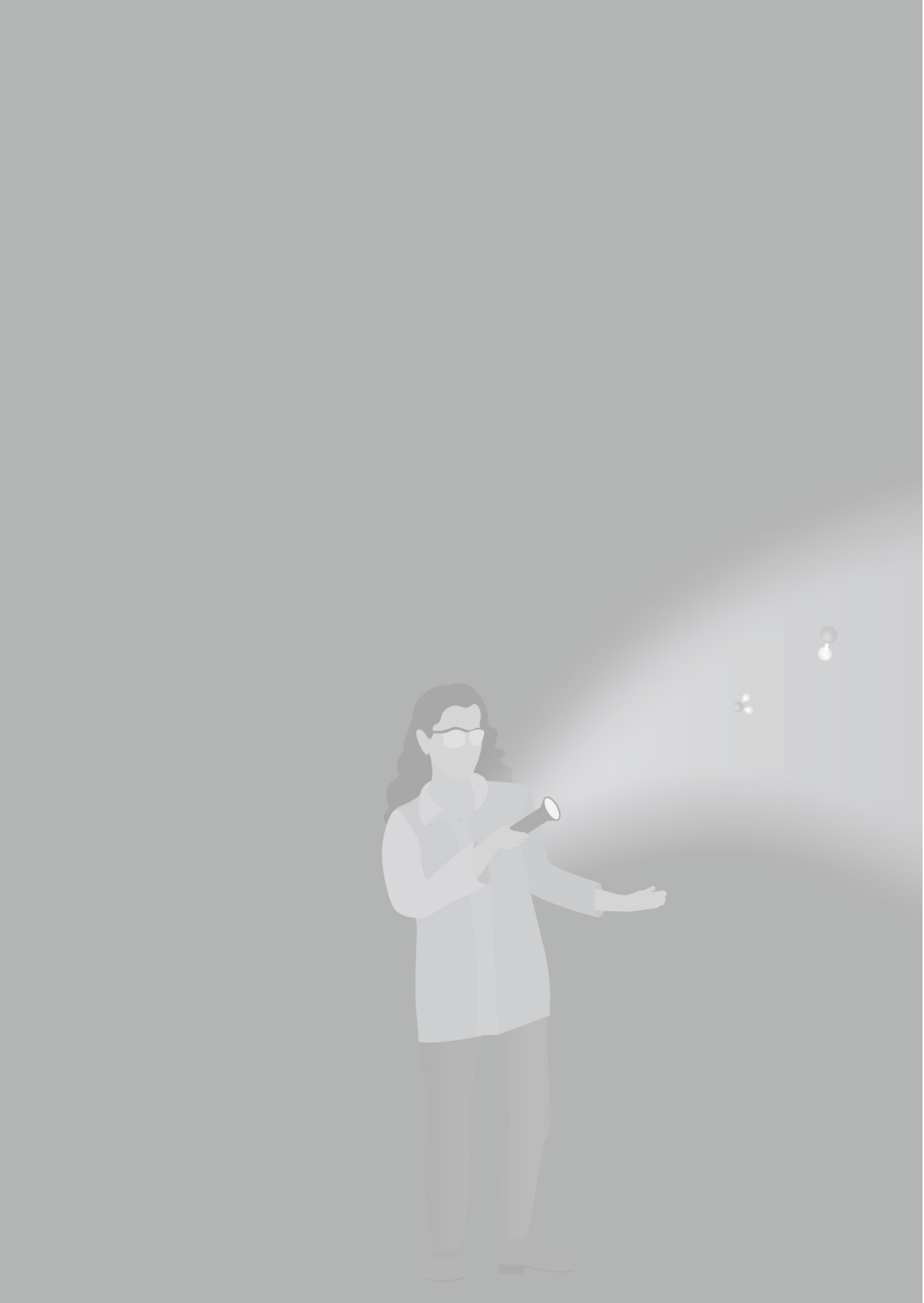

Appendix C
Supporting Information to Chapter 4

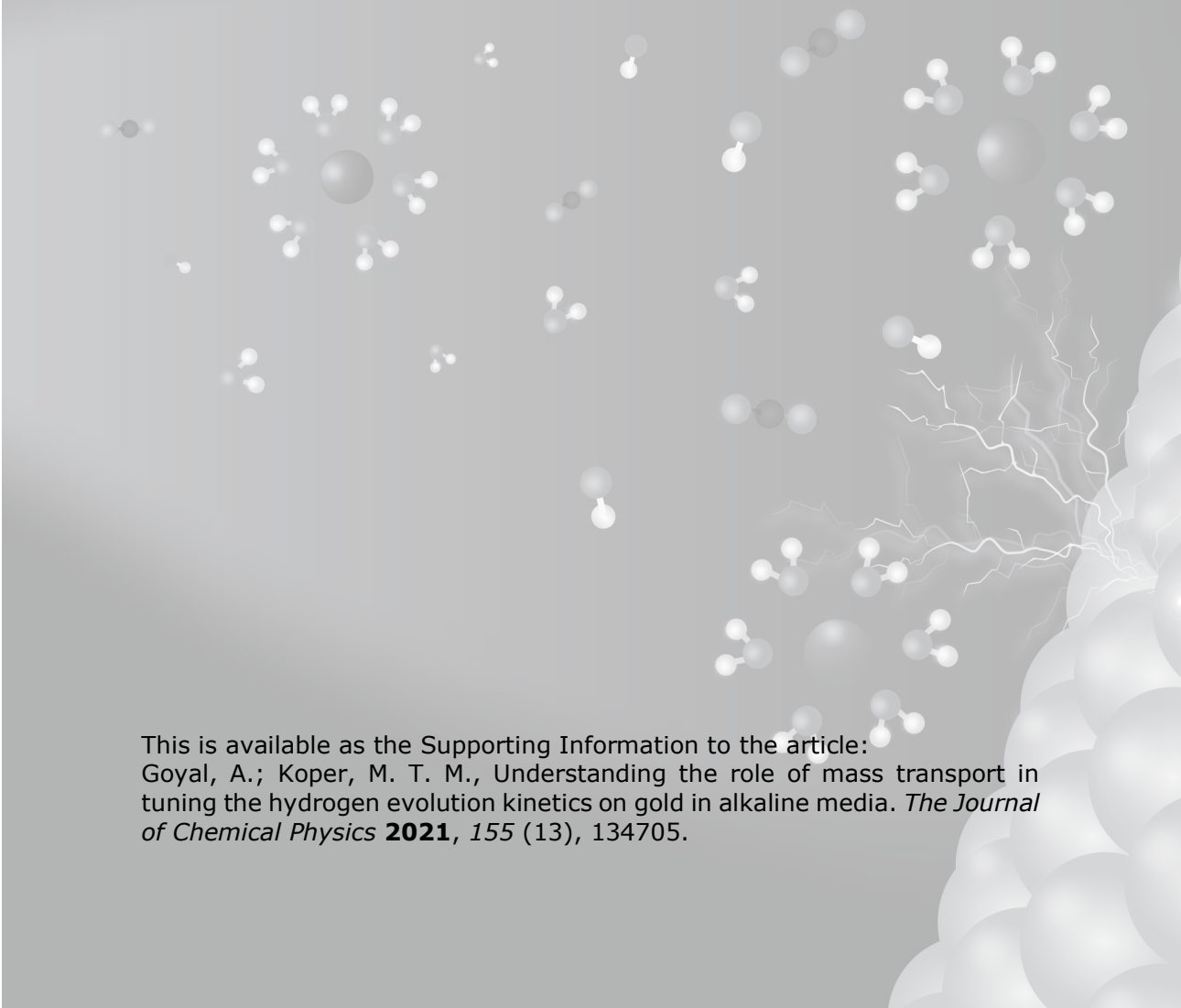

This is available as the Supporting Information to the article:
Goyal, A.; Koper, M. T. M., Understanding the role of mass transport in tuning the hydrogen evolution kinetics on gold in alkaline media. *The Journal of Chemical Physics* **2021**, *155* (13), 134705.

S1. Analytical model for the HER kinetics on Au electrodes

Here, we will present a simple model for the rate of hydrogen evolution reaction that can semi-quantitatively explain the experimental data presented in the main manuscript. The model is based on the idea that the rate of HER depends on the local (interfacial) concentration of cations, in the sense that the cations near the surface, essentially in the (outer-)Helmholtz plane, promote the hydrogen evolution.
We assume that the rate of the water reduction reaction:

$$2\ H_2O + 2\ e^- \rightarrow H_2 + 2\ OH^- \qquad \text{(S1)}$$

is determined by the first step, as suggested by the experimental Tafel slope:

$$H_2O + e^- + * \rightarrow *H + OH^- \qquad \text{(S2)}$$

where * is a free site on the surface and *H is a hydrogen atom adsorbed on that site. First, we will assume that all sites on the surface are equivalent and that there are no lateral interactions between the adsorbed hydrogens (Langmuir model). We will also assume that the rate of this reaction depends on the local concentration of cations because the cation can favorably interact with the transition state of the reaction. In a formal equation, this promoting action of the cation can be written as:

$$H_2O + e^- + * + cat^+ \rightarrow *H\ \text{--}\ OH^{\delta-}\text{--}cat^+ + (1-\delta)\ e^- \rightarrow *H + OH^- + cat^+ \qquad \text{(S3)}$$

The idea is that the cation interacts favorably with the transition state because a (partially) negatively hydroxide is being split off from the reacting water molecule. This model is very similar to a model suggested recently by our group in which the hydroxide is (transiently) stabilized by an oxophyllic adatom on the platinum electrode.[1] The key assumptions of the suggested rate equation are that it depends only on the concentration of cations near the surface, not directly on the electrolyte pH, and that this dependence follows a power law:

$$v_1 = k_1^{eff0} exp\left(-\frac{\alpha FE}{RT}\right)[Cat^+]_s^{\gamma} \qquad \text{(S4)}$$

where, k_1^{eff0} is the standard rate constant, α is the transfer coefficient ($\alpha = 0.5$), F is Faraday's constant (96485 C mol^{-1}), E is the applied potential with respect to the standard potential of the reaction, R is the universal gas constant (8.314 J K^{-1} mol^{-1}), T is the temperature (K), $[Cat^+]_s$ is the surface concentration of cations (in mol cm^{-3}) and γ is the (empirical) reaction order in the cation concentration.
Moreover, under the steady-state conditions, the OH^- generation rate (i.e. HER rate) must be equal to its diffusion rate:

$$k_1^{eff0} exp\left(-\frac{\alpha FE}{RT}\right)[Cat^+]_s^{\gamma} = \frac{D_{OH^-}}{\delta_{OH^-}}([OH^-]_s - [OH^-]_b) \quad \text{(S5)}$$

where δ_{OH^-} is the diffusion layer thickness ($\delta_{OH^-} = 1.61 \times D_{OH^-}^{\frac{1}{3}} \times \nu^{\frac{1}{6}} \times \omega^{-\frac{1}{2}}$), D_{OH^-} is the diffusion coefficient of OH^- (5.273×10^{-5} cm^2/s), ν is the kinematic viscosity of water (8.9×10^{-3} cm^2/s) and ω is the angular frequency of rotation (in rad/s), $[OH^-]_s$ is the surface concentration of hydroxyl ions (in mol cm^{-3}) and $[OH^-]_b$ is the bulk concentration of hydroxyl ions (in mol cm^{-3}).
The conservation of electro-neutrality with in the diffusion layer (which is a reasonable assumption except for the double-layer region very close to the surface ≤ 10 Å) requires that:

$$[OH^-]_s + [ClO_4^-]_s = [Cat^+]_s \quad \text{(S6)}$$

Therefore, the increase in the concentration of OH^- at the surface must be accompanied by a corresponding increase in the concentration of cations, which we assume to be linear, i.e.

$$[Cat^+]_s = [Cat^+]_b + \beta([OH^-]_s - [OH^-]_b) \quad \text{(S7)}$$

where β is a kind of local transference number:

$$\beta = \frac{u_{Cat^+}[Cat^+]_b}{u_{Cat^+}[Cat^+]_b + u_{ClO_4^-}[ClO_4^-]_b} = \frac{D_{Cat^+}[Cat^+]_b}{D_{Cat^+}[Cat^+]_b + D_{ClO_4^-}[ClO_4^-]_b} \quad \text{(S8)}$$

$$\left(\text{where } u = \frac{|z|FD}{RT} \text{ as derived from Nernst} - \text{Einstein relationship}\right)$$

Hence, eqn. S5 can be re-written by substituting the expression for $[Cat^+]_s$ from eqn. S7 as follows:

$$k_1^{eff0} exp\left(-\frac{\alpha FE}{RT}\right)([Cat^+]_b + \beta([OH^-]_s - [OH^-]_b))^{\gamma} = \frac{D_{OH^-}}{\delta_{OH^-}}([OH^-]_s - [OH^-]_b) \quad \text{(S9)}$$

There is no general analytical solution for this equation, but we can use a first-order Taylor expansion to re-write the term $([Cat^+]_b + \beta([OH^-]_s - [OH^-]_b))^{\gamma}$ as follows:

$$([Cat^+]_b + \beta([OH^-]_s - [OH^-]_b))^{\gamma} \approx [Cat^+]_b{}^{\gamma-1}([Cat^+]_b + \gamma\beta([OH^-]_s - [OH^-]_b)) \quad \text{(S10)}$$

where we have assumed that $[Cat^+]_b \gg \beta([OH^-]_s - [OH^-]_b)$. Then by using eqn. S10 we can solve eqn. S9 for $[OH^-]_s$ as follows:

$$[OH^-]_s = [OH^-]_b + \frac{k_1^{eff0} exp\left(-\frac{\alpha FE}{RT}\right)[Cat^+]_b{}^{\gamma}}{\left(\frac{D_{OH^-}}{\delta_{OH^-}} - \gamma\beta k_1^{eff0} exp\left(-\frac{\alpha FE}{RT}\right)([Cat^+]_b)^{\gamma-1}\right)} \quad \text{(S11)}$$

As a result, the final current for HER can be calculated as follows:

$$j_{HER} = -2Fk_1^{eff0} exp\left(-\frac{\alpha FE}{RT}\right)\left([Cat^+]_b + \beta\left(\frac{k_1^{eff0} exp\left(-\frac{\alpha FE}{RT}\right)[Cat^+]_b{}^{\gamma}}{\left(\frac{D_{OH^-}}{\delta_{OH^-}} - \gamma\beta k_1^{eff0} exp\left(-\frac{\alpha FE}{RT}\right)([Cat^+]_b)^{\gamma-1}\right)}\right)\right)^{\gamma} \quad \text{(S12)}$$

Here, the eqns. have been written by assuming that the central parameter that affects the kinetics of HER on Au electrodes is only the near surface cation concentration ($[Cat^+]_s$) and the rotation dependence of HER kinetics is a byproduct of the associated changes in the near-surface cation concentration with the changing surface pH. In the simulations we take the standard rate constant for the reaction, i.e. k_1^{eff0} to be 10^{-9} cms^{-1}, since Au is a bad catalyst for HER.[2] However, we note, that the values of the intrinsic rate constant can depend on the identity of the cation in the electrolyte, but for the sake of simplicity we neglect these effects in our simulations. Moreover, we take γ to be 0.5 in the simulations since the model is meant to represent the promotional regime of cations for HER and based on our experimental results (Figure 3) we expect the reaction order in cation concentration to be a positive fractional value. Additionally, based on the theoretically calculated values of β for the different alkali metal cations (Table S1) we take β to be 0.5 in the simulations.

S2. Supplementary figures

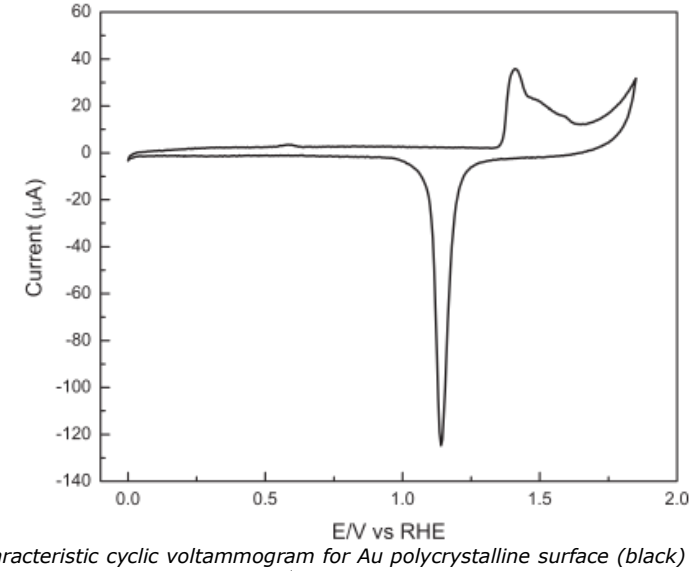

Figure S1 Characteristic cyclic voltammogram for Au polycrystalline surface (black) obtained in 0.1 M H_2SO_4 in Ar sat. environment at 50 mVs^{-1} where the electrochemically active surface area (ECSA) was calculated by integrating the area of the Au_xO_y reduction peak in the scan.

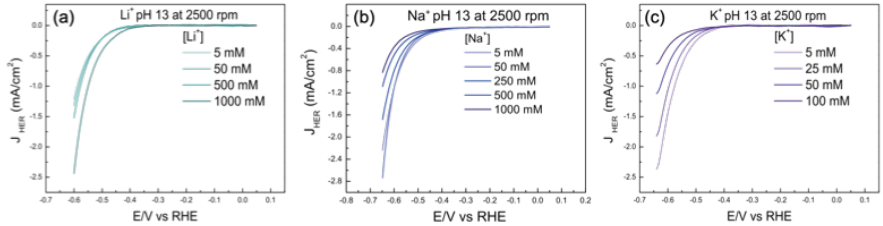

Figure S2 Experimentally obtained negative going scan of the cyclic voltammogram at polycrystalline Au electrodes at pH 13 and 2500 rpm for (a) Li^+, (b) Na^+ and (c) K^+ at different bulk cation concentrations. The experimentally obtained reaction orders from these measurements are shown in Fig. 3d, e and f in the main manuscript.

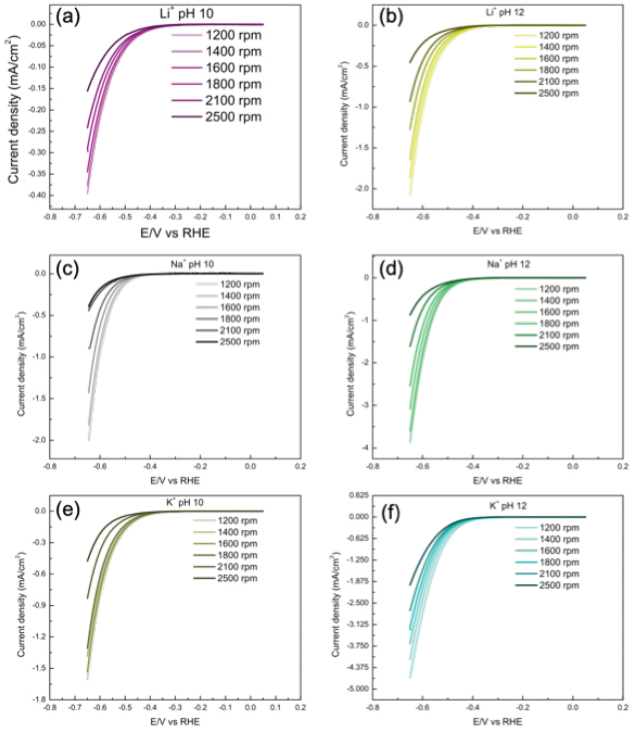

Figure S3 Negative going scan of the cyclic voltammograms obtained for HER on Au polycrystalline surface in Li^+ ion containing electrolytes at (a) pH 10 and (b) pH 12, in Na^+ ion containing electrolytes at (c) pH 10 and (d) pH 12, and in K^+ ion containing electrolytes at (e) pH 10 and (f) pH 12 at a fixed cation concentration in the bulk (0.1 M) at different rotation rates (2500 rpm, 2100 rpm, 1800 rpm, 1600 rpm, 1400 rpm and 1200 rpm) at a scan rate of 25 mVs^{-1}.

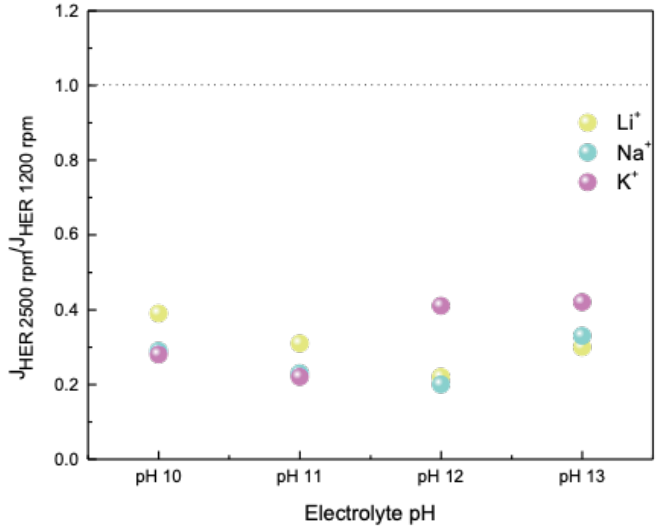

Figure S4 Ratio of the HER current density at 2500 rpm/ 1200 rpm at -0.65 V (vs RHE) as a function of the electrolyte pH for Li^+, Na^+ and K^+ ion containing electrolytes. A ratio lower than one indicates that the HER current density is higher at 1200 rpm than 2500 rpm. Lower values of the ratio indicate that the difference between the current density at 1200 rpm and 2500 rpm is larger.

Table S4 The local transference number (β) as derived from eqn. S8.

Cation	$\beta = \frac{D_{Cat^+}[Cat^+]_b}{D_{Cat^+}[Cat^+]_b + D_{ClO_4^-}[ClO_4^-]_b}$
Li^+	0.37
Na^+	0.45
K^+	0.52

References

1. McCrum, I. T.; Koper, M. T. M., The role of adsorbed hydroxide in hydrogen evolution reaction kinetics on modified platinum. *Nature Energy* **2020,** *5* (11), 891-899.
2. Bard, A. J.; Faulkner, L. R., *Electrochemical methods : fundamentals and applications* Wiley: New York, **1980**.

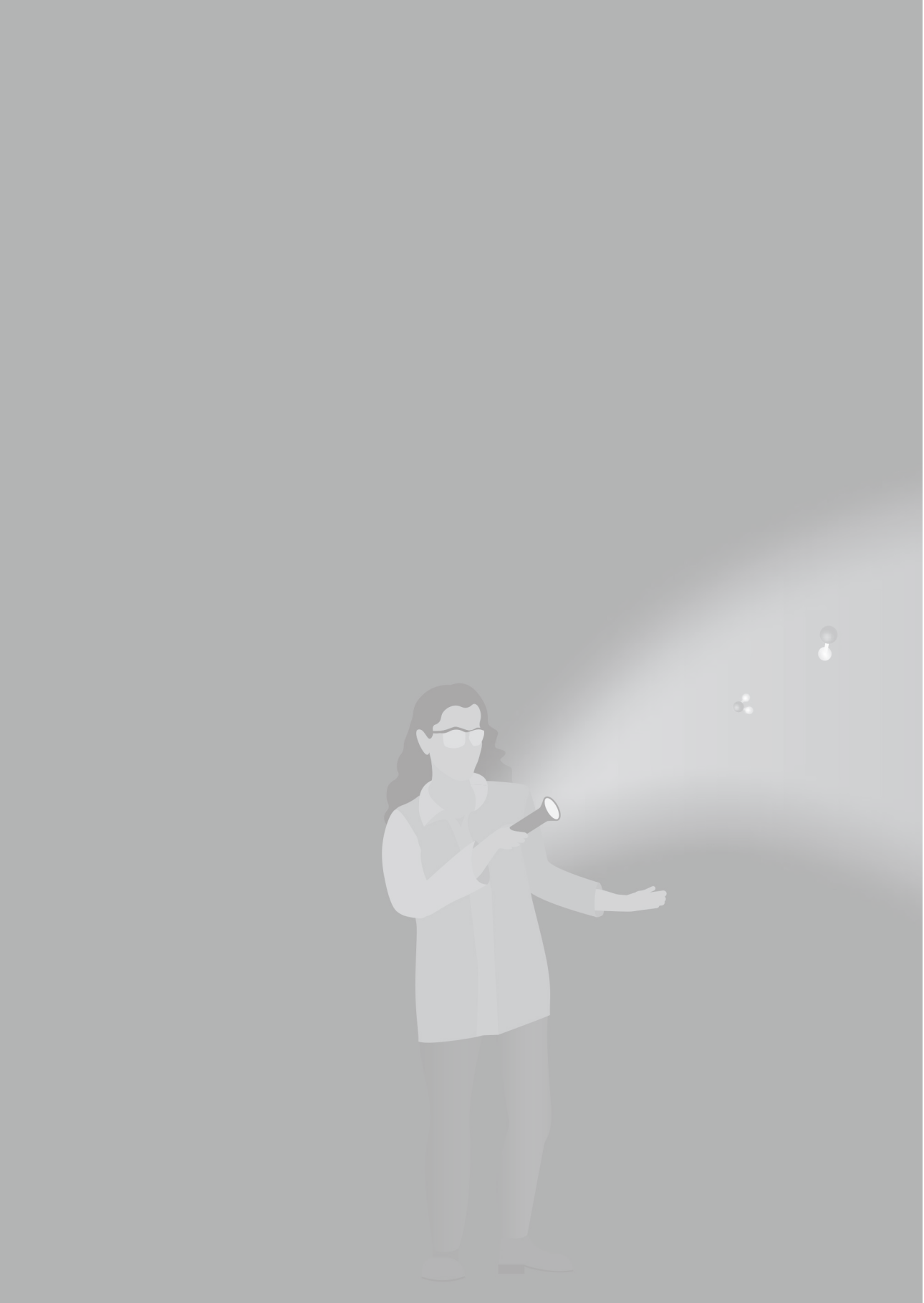

Appendix D
Supporting Information to Chapter 5

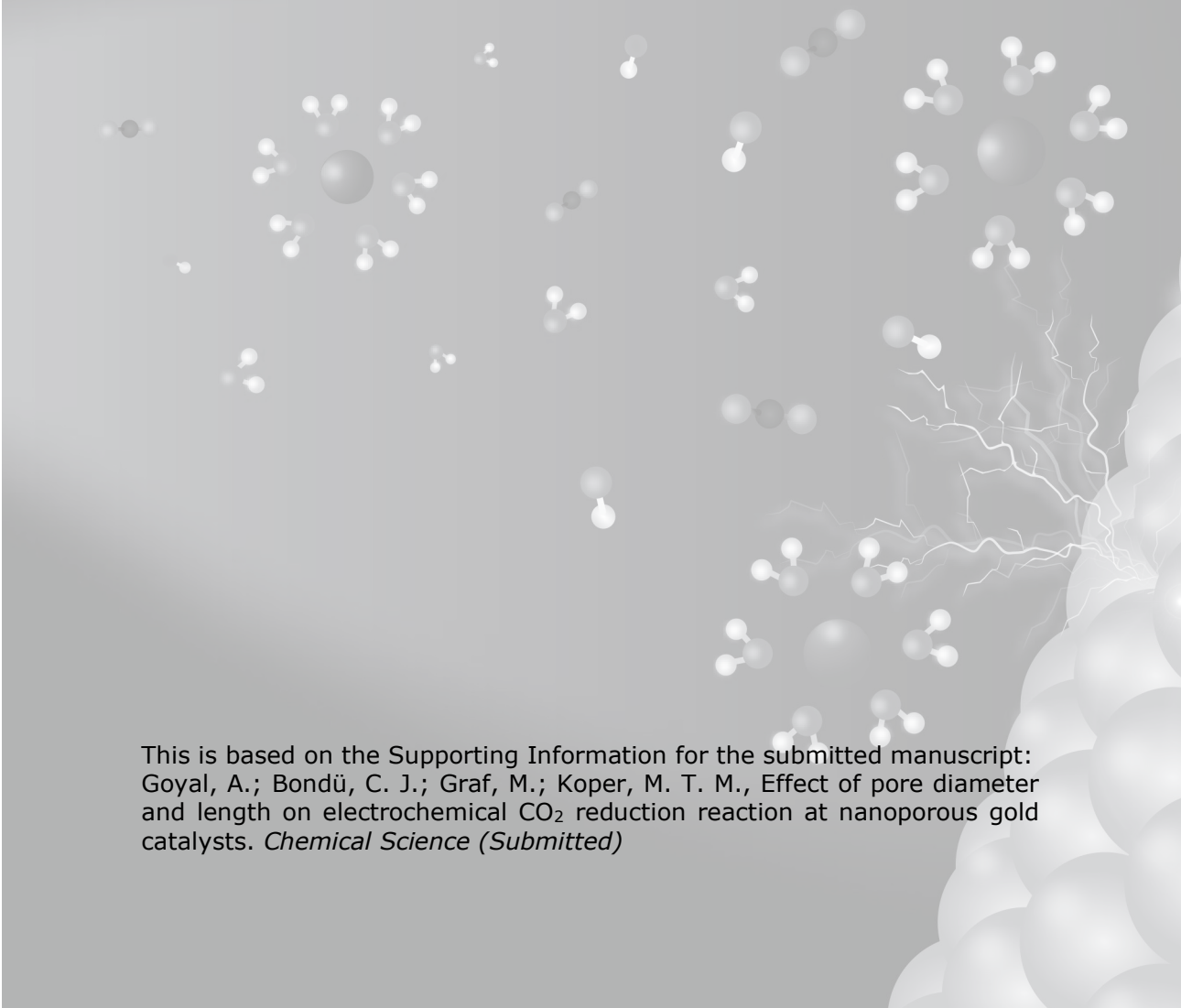

This is based on the Supporting Information for the submitted manuscript: Goyal, A.; Bondü, C. J.; Graf, M.; Koper, M. T. M., Effect of pore diameter and length on electrochemical CO_2 reduction reaction at nanoporous gold catalysts. *Chemical Science (Submitted)*

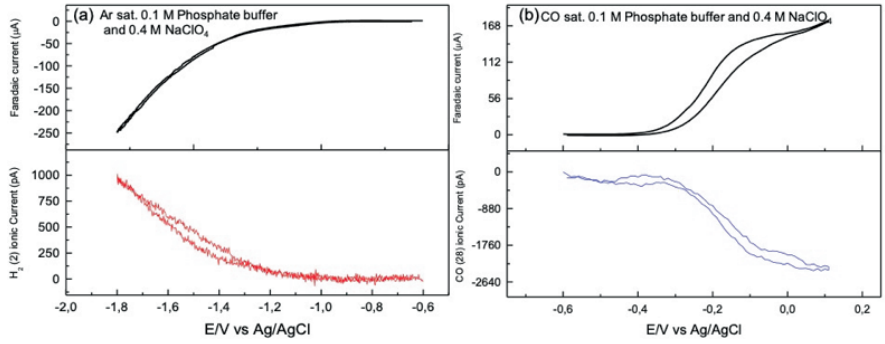

Figure S2 DEMS calibration experiment for (a) H_2 and (b) CO, performed in 0.1 phosphate buffer and 0.4 M $NaClO_4$ at 5 mVs^{-1} and a flow rate of 300 $\mu Lmin^{-1}$ in Ar sat. and CO sat. conditions respectively. For determining $K^{\circ}_{H_2}$ the Faradaic current for HER and the ionic current at m/z 2 as shown in S1a in the top panel and the bottom panel, respectively, were plugged into eqn. 3 (see Section 2.4 in the Main Manuscript) where z was taken to be 2. For determining K°_{CO} the Faradaic current for CO oxidation and the ionic current at m/z 28 as shown in S1b in the top panel and the bottom panel, respectively, were plugged into eqn. 3 (see Section 2.4 in the Main Manuscript) where z was taken to be 2.

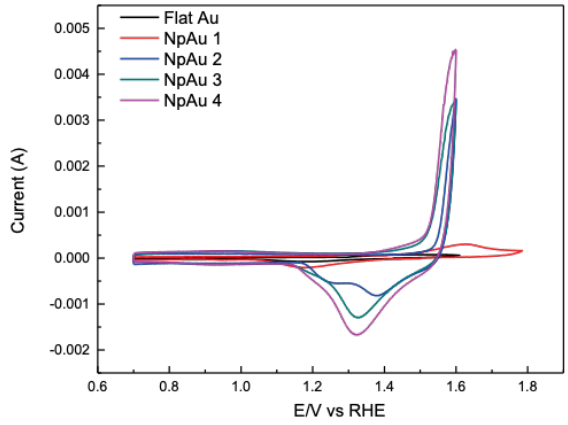

Figure S3 Characterization cyclic voltammograms for different Au catalysts in 0.1 M H_2SO_4 in Ar sat. environment at 50 mVs^{-1} where the charge of the Au_xO_y reduction peak was used to calculate the electrochemically active surface area (ECSA) of the different samples

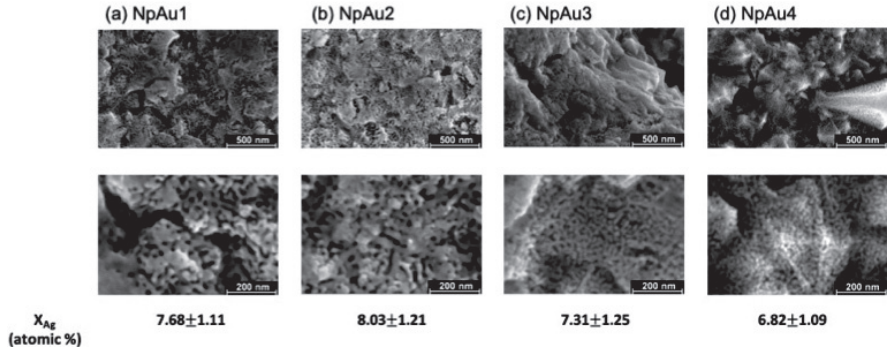

Figure S4 SEM characterization of different nano-porous Au (NpAu) samples, left to right: (a) NpAu1, (b) NpAu2, (c) NpAu3 and (d) NpAu4 where the upper row shows the low magnification SEM images and the lower row shows the high magnification SEM images for the different samples. At the bottom, the residual Ag content (X_{Ag}) as determined by the EDX measurements at low magnification is given for every NpAu sample along with the internal quantification error.

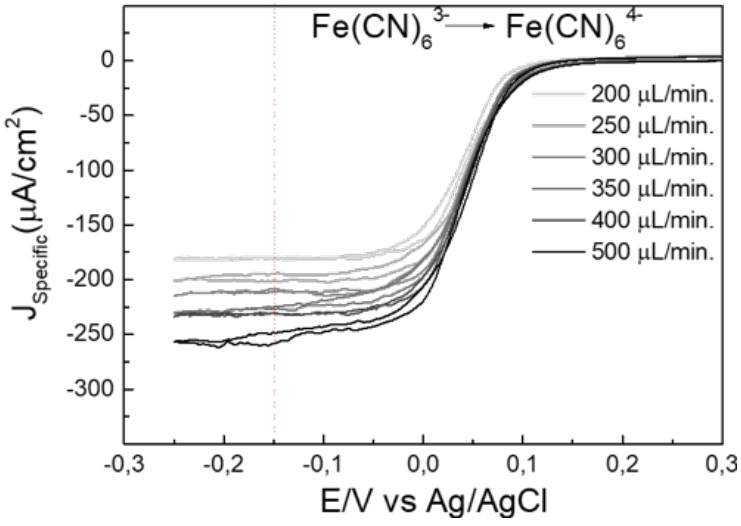

Figure S5 Determination of the diffusion layer thickness in the dual thin layer cell: cyclic voltammograms obtained in 0.1 M $NaHCO_3$ and 0.4 M $NaClO_4$ with 10 mM $K_3Fe(CN)_6$ at a scan rate of 5 mVs^{-1}, at different flow rates, where the diffusion limited currents for ferricyanide reduction at -0.15 V vs Ag/AgCl (indicated by the dotted line) were used to calculate the diffusion layer thickness by using Fick's law.

Table S1 Diffusion layer thickness (middle column) at different flow rates as calculated from the data shown in Figure S4 by using Fick's first law of diffusion, where no. of electrons involved were taken to be 1, concentration of $K_3Fe(CN)_6$ was taken to be 10 mM, diffusion coefficient of $Fe(CN)_6^{3-}$ was taken to be 7×10^{-6} cm^2s^{-1} and Faraday's constant was taken to be 96485 $Cmol^{-1}$. Thereafter, the theoretical diffusion limited current for CO2RR under the condition of our studies was calculated (right most column) by again using Fick's law where no. of electrons involved in the reaction were taken to be 2 and the concentration of CO_2 (aq.) was taken to be 16.5 mM (0.5 atm. CO_2) and the values for the diffusion layer thickness were taken from the middle column of the table.

Flow rate (μ L/min)	Diffusion layer thickness (μm)	$J_{Limiting\ (theoretical)}$ (mA/cm^2) at 0.5 atm. CO_2
200	374.80719	-1.40061
250	336.0546	-1.56213
300	323.70757	-1.62171
350	297.23011	-1.76617
400	293.23413	-1.79024
500	261.41034	-2.00818

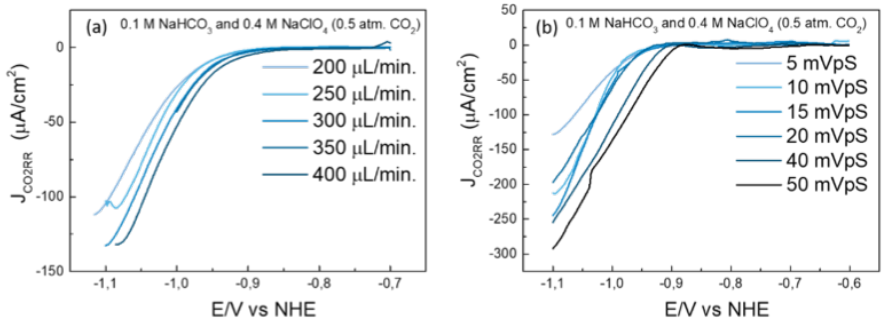

Figure S6 Partial current density for CO formation on Flat Au as obtained from the ionic current at m/z 28 by using eqn. 3 (in the main manuscript) with 0.5 atm. of CO_2 in 0.1 M $NaHCO_3$ and 0.4 M $NaClO_4$ containing electrolyte at (a) different flow rates and (b) different scan rates

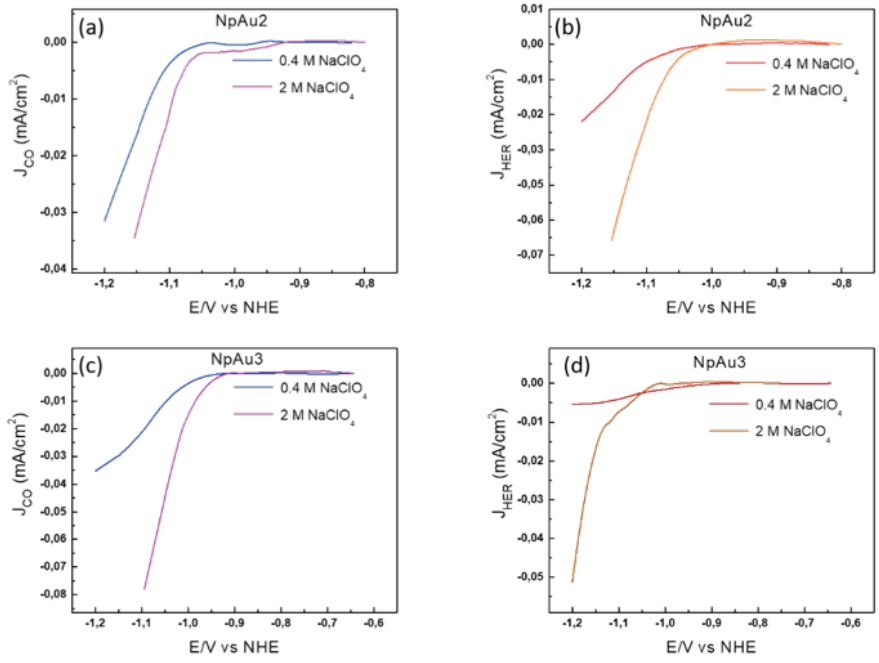

Figure S7 Partial specific current density for CO formation as obtained from the ionic current at m/z 28 by using eqn. 3 (Main Manuscript) with 0.5 atm. CO_2 in 0.1 M $NaHCO_3$ and 0.4 M $NaClO_4$ containing electrolyte (blue) and in 0.1 M $NaHCO_3$ and 2 M $NaClO_4$ containing electrolyte (purple) at a scan rate of 5 mVs^{-1} and a flow rate of 300 $\mu Lmin^{-1}$ on (a) NpAu2 and (c) NpAu3 and Partial current density for HER as obtained from the ionic current at m/z 2 by using eqn. 3 (Main Manuscript) with 0.5 atm. CO_2 in 0.1 M $NaHCO_3$ and 0.4 M $NaClO_4$ containing electrolyte (red) and in 0.1 M $NaHCO_3$ and 2 M $NaClO_4$ containing electrolyte (orange) at a scan rate of 5 mVs^{-1} and a flow rate of 300 $\mu Lmin^{-1}$ on (b) NpAu2 and (d) NpAu 3.

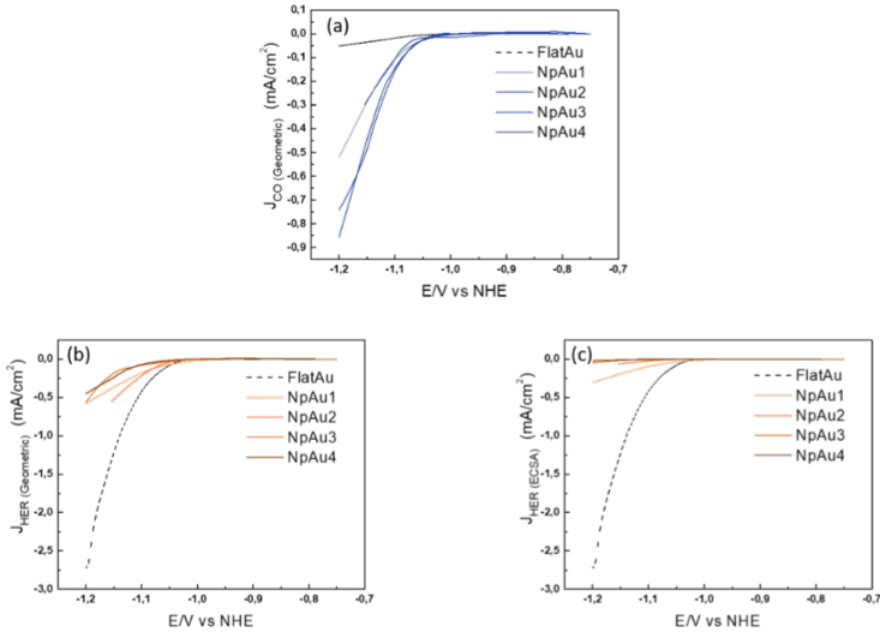

Figure S8 (a) Partial geometric current density for CO formation on different Au catalysts as obtained from the ionic current at m/z 28 by using eqn. 3 (Main Manuscript) with 0.5 atm. CO_2 in 0.1 M $NaHCO_3$ and 2 M $NaClO_4$ containing electrolyte at a scan rate of 5 mVs^{-1} and a flow rate of 300 $\mu Lmin^{-1}$. (b) Partial geometric current density for HER and (c) Partial specific current density for HER, as obtained from the ionic current at m/z 2 by using eqn. 3 (Main Manuscript) with 0.5 atm. CO_2 in 0.1 M $NaHCO_3$ and 2 M $NaClO_4$ containing electrolyte at a scan rate of 5 mVs^{-1} and a flow rate of 300 $\mu Lmin^{-1}$.

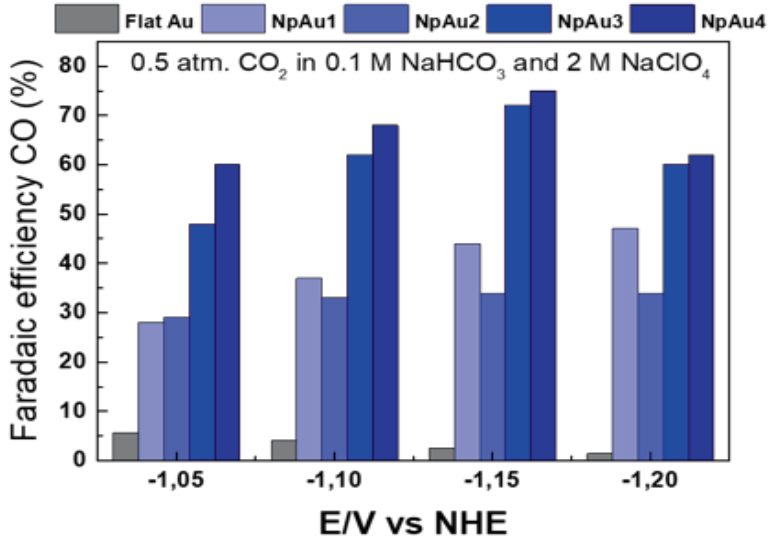

Figure S9 Faradaic efficiency for CO formation of the different Au catalysts in 0.5 atm. CO_2 and 0.1 M $NaHCO_3$, 2 M $NaClO_4$ containing electrolyte at different potentials (vs. NHE) as obtained from the DEMS measurements by using eqn. 4 (Main Manuscript).